Modelling the diffuse TeV γ-ray emission in the Galactic Center

Bachelorarbeit aus der Physik

vorgelegt von

Martin Schneider

Tag der Abgabe: 30. Juli 2019

Friedrich-Alexander-Universität Erlangen-Nürnberg

1. Gutachter: Prof. Dr. Christopher van Eldik
2. Gutachter: Prof. Dr. Stefan Funk

Abstract

The very high energy diffuse γ-ray emission in the Galactic Center was observed to roughly follow the dense matter distribution in the central molecular zone. This thesis explores a possible scenario for the origin of the diffuse emission. The general assumption is that the TeV γ-rays emerge from interactions of the ambient molecular matter in the Galactic Center and diffusing cosmic rays. These cosmic rays are assumed to originate from a more active past of the super-massive black hole Sgr A* 10^7 years ago. In this thesis an existing simulation of this process is build upon that assumes the diffusion of protons in a purely turbulent magnetic field of $50\,\mu\mathrm{G}$. These protons are distributed according to a power law with a spectral index of $\Gamma_p = 2$ and tracked over the period of 10^7 years. The resulting γ-ray flux map has a spectral index of ≈ 2.26, coinciding with a recent H.E.S.S. analysis. It is then used as a diffuse model component for the analysis of H.E.S.S 1 observations. The simulation can reproduce the characteristics of the observed emission in general with the exception of an excess at 1.25° longitude and -0.15° latitude near the center of Sgr D that might be an unknown source.

Contents

1 Introduction

γ-ray astronomy is the astronomical observation of photons with the highest energies. These photons are created in regions where particles are accelerated to very high energies e.g. supernova remnants, but also the center of the Milky Way. Compared to charged particles γ-rays are not deflected by magnetic fields when passing through the Galaxy, thus pointing back directly at their origin when observed. In order to detect very-high-energy (VHE) γ-rays with photon energies between 100 GeV and 100 TeV Imaging Air Cherenkov Telescopes (IACTs) are used. As the name implies the telescope works by imaging a short flash of Cherenkov radiation, which is created by a shower of relativistic charged particles when a VHE γ-ray hits the atmosphere.

Located in the southern hemisphere, the H.E.S.S ("High Energy Stereoscopic System") array is an IACT system that provides excellent observation conditions for VHE γ-ray sources such as the Galactic Center region. Apart from the two most dominant sources of VHE γ-rays located in that region, the central super-massive black hole Sagittarius A* (Sgr A*) and the pulsar wind nebula G 0.9+0.1, the surrounding molecular clouds as well as the diffuse γ-ray emission associated with it have become a subject of current research.

Currently a promising scenario for the origin of the observed diffuse γ-ray emission is the interaction of cosmic rays with the matter in the molecular clouds. Unlike the name suggests, cosmic rays are actually high-energy particles with intrinsic mass such as protons and muons. At first it was proposed that the cosmic rays originate from a supernova explosion around 10^4 years ago [Aharonian et al., 2006], but further research on this topic suggests a more active past of the super-massive black hole Sgr A* over the last 10^6 to 10^7 years as the source of these high-energy particles [HESS Collaboration et al., 2016]. In this context Sgr A* is often called a 'PeVatron' (short for petaelectronvolt accelerator).

One approach to achieve an interaction between the cosmic rays and the matter in the central molecular zone is to let the cosmic rays diffuse away from the center. The hardness of the γ-ray spectrum and the condition in the molecular clouds indicate that the diffuse γ-ray emission is more likely to be produced by nuclei or protons, rather than electrons [Aharonian et al., 2006]. With that in mind, the hadronic diffusion scenario can be tested by diffusing charged particles in a turbulent magnetic field and calculating the resulting emission from the interaction of these particles with ambient matter.

This bachelor thesis aims to model the diffuse γ-ray emission based on the simulation approach by Ziegler (2014) to assess the validity of the hadronic diffusion scenario. In Chapter 2, a recent characterisation of the diffuse γ-ray emission made with the H.E.S.S. experiment is shown. In Chapter 3, the used model is explained in detail and the refined distinctions to the developed python-version of the code written by Wong (2019) are presented. In Chapter 4, the simulated γ-ray emission is then used as a model for the diffuse emission in the Galactic Center and fit to H.E.S.S 1 data. The obtained results are then used to analyse the diffuse emission model for different energy regimes. At last, in Chapter 5, a brief summary and outlook is given.

2 H.E.S.S Observations of diffuse γ-ray emission in the Galactic Center

A recent H.E.S.S analysis of the Galactic Center by H. E. S. S. Collaboration et al. (2018) has shown that the emission correlated with the dense matter in the central molecular zone follows its distribution, while accounting for half of the total diffuse emission flux. After subtraction of the two main point sources in the Galactic Center the super-massive black hole Sgr A* and the pulsar wind nebula G 0.9+0.1, the observations are dominated by the remaining dense gas component. The stages of the iterative fitting process to test for a variety of contributions to the observed γ-ray emission are shown in Figure 1.

The noticeable dip in γ-ray emission at about 1° longitudinal distance from the Galactic Center is predicted to be caused by two effects. These are a more diffuse matter distribution along the line-of-sight axis, supported by the face-on view of the central molecular zone presented by Sawada et al. (2004) and a declining cosmic-ray density towards the outer regions.

Interestingly an additional large-scale emission component is found by H. E. S. S. Collaboration et al. (2018) with a larger extension in latitude. This component is needed to reproduce the observed morphology. Further contributions are likely to originate from more dense structures or unresolved sources.
Also worth noting is the big central component in the center that indicates a cosmic-ray accelerator at the very centre of the Galaxy. This hypothesis is also supported by HESS Collaboration et al. (2016) as their findings suggest that Sgr A* is a possible candidate for a PeVatron, although its current rate of particle acceleration is not sufficient. Looking at these results the idea of the hadronic diffusion scenario is pursued by developing a diffuse emission model and comparing it to H.E.S.S 1 data.

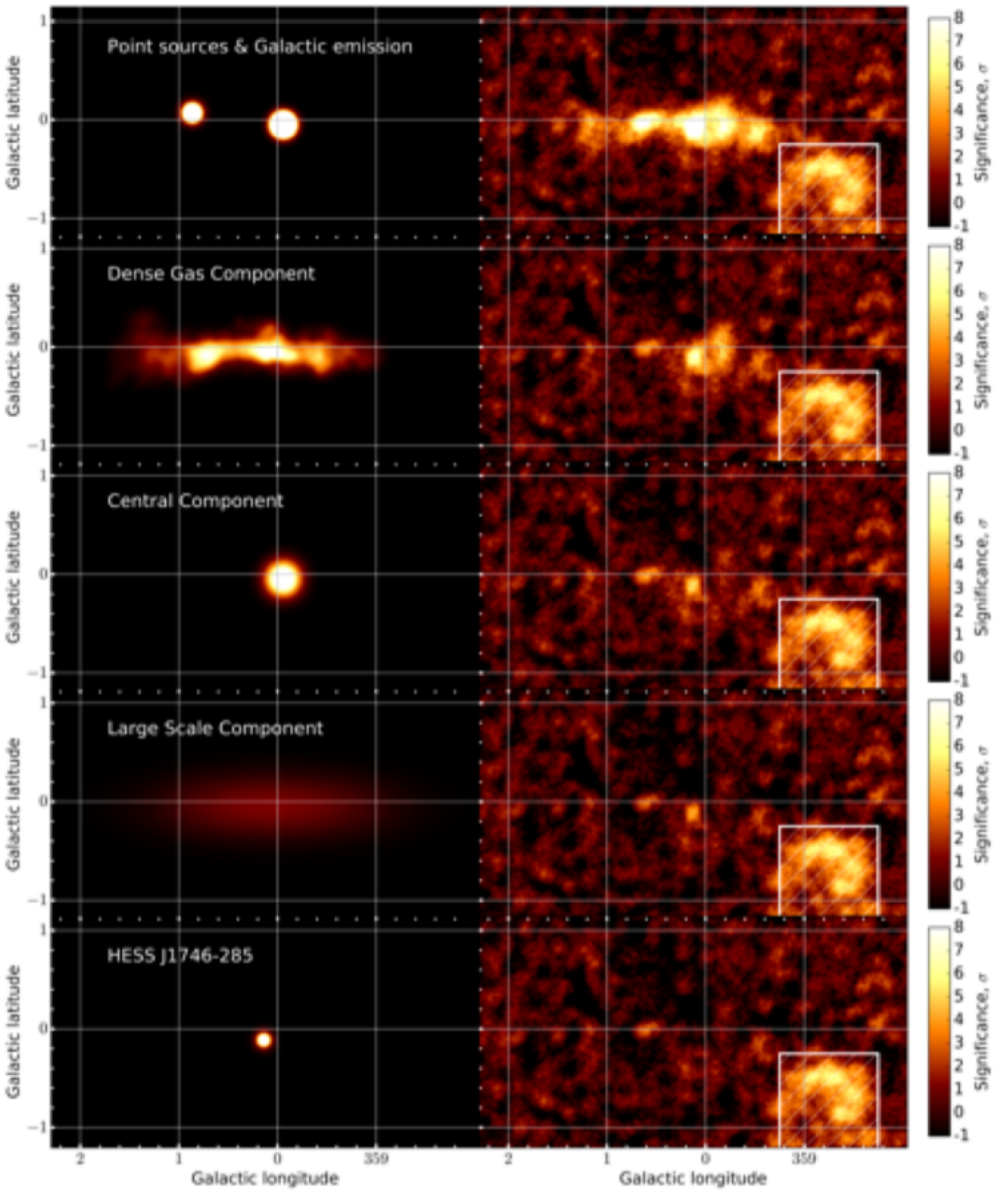

Figure 1: The steps of the iterative fitting process are presented with the added model count map of each component on the left and the corresponding residual significance map on the right. The model count maps are correlated with the H.E.S.S point spread function (PSF) and given in counts per pixel whereas the significance maps are given in units of significance level. The Li & Ma significance maps use the correlated model map as background and the data counts map as signal (picture taken from H. E. S. S. Collaboration et al. 2018).

3 Modelling approach for the diffuse γ-ray emission in the Galactic Center

The modelling approach in this thesis is based on the scenario that charged hadronic particles are accelerated by a central source and diffuse out into the ambient space under a purely turbulent magnetic field. A first step to simulate this process has already been done by Ziegler (2014). Based on this work a python-version of the simulation was developed by Wong (2019) in order to improve computation time with the final goal to reproduce an emission as observed with the H.E.S.S instrument for a simulation time scale of 10^7 years. The output of the code features a γ-ray flux map with an energy axis, which is required for a later fitting to H.E.S.S 1 data using the `gammapy`-package for python.

3.1 The model idea

The simulation code used in this thesis was implemented by Wong (2019) and roughly follows the approach by Ziegler (2014). To briefly summarize the simulation procedure its concept can be split in three steps. The charged hadronic particles responsible for the diffuse emission in the Galactic Center will be represented by protons.
Since the idea is to produce the γ-ray flux by interaction with these particles, the first step is to initialize a number of protons in the central bin and distribute them. This is set up, so that the differential energy spectrum of the protons follows a power law

$$\frac{\mathrm{d}N_p\left(E_p\right)}{\mathrm{d}\left(E_p\right)} \propto \left(E_p\right)^{-2} \tag{1}$$

where E_p denotes the proton energy and $\mathrm{d}N_p\left(E_p\right)$ the number of protons in the energy interval $(E_p,\, E_p + \mathrm{d}E_p)$. Following that in step two, the diffusion process for the protons is calculated using the diffusion coefficients for $50\,\mu\mathrm{G}$ to obtain a Gaussian spread proton distribution. Finally in step three a γ-ray flux-map is produced. This is done by multiplying the density map of the molecular clouds in the Galactic Center with the proton distribution element wise. After that a look-up table is used to finally convert the number of protons at a certain energy with its density value into γ-ray flux. The full γ-ray spectrum produced by the protons of the entire energy range of $10^{-1}\,\mathrm{TeV}$ to $10^{5}\,\mathrm{TeV}$ is obtained by a summation over the γ-ray spectra resulting from the individual energy bins of the proton spectrum.

3.2 The diffusion process

The high-energy protons are assumed to diffuse away from the center due to their interactions with the surrounding turbulent magnetic field. When a time dependent source term and energy losses or gains are neglected the diffusion equation for this problem assuming scalar and constant diffusion is given by [see Ziegler, 2014]

$$\frac{\partial n(E,r,t)}{\partial t} = D(E)\nabla^2 n(E,r,t) \tag{2}$$

with $n(E,r,t)$ being the number density of particles and $D(E)$ being the diffusion coefficient.

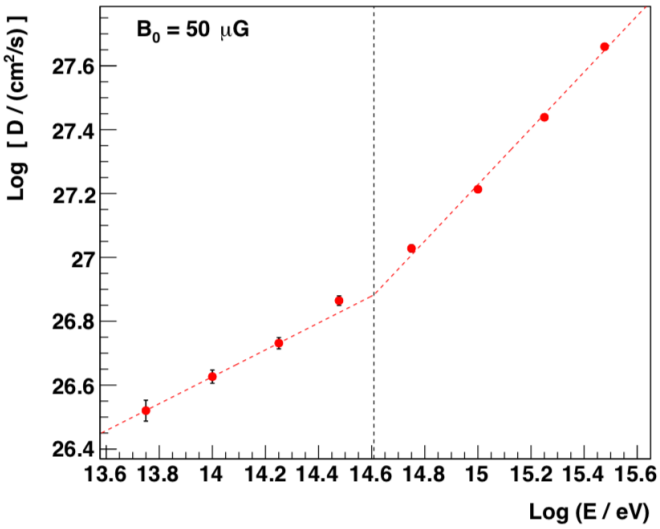

Figure 2: Derived results for the diffusion coefficient $D(E)$ for $B_0 = 50\,\mu\text{G}$. The data points exhibit a break in the linear scaling of $\log(D)$ as well as the diffusion coefficient as a function of $\log(E)$. The red dashed curves represent linear fit curves to the data, the vertical dashed line indicates the position of the break (picture taken from Ziegler (2014)).

Using the solution to Equation 2 for N_0 particles ejected at the origin at $t = 0$ [see Bakunin, 2008]

$$n(E,r,t) = \frac{N_0}{[4\pi D(E)t]^{\frac{3}{2}}} \exp\left(-\frac{r^2}{4D(E)}t\right) \tag{3}$$

the marginal probability density function along each spatial axis $r_i = x, y, z$ found by Ziegler (2014) is a Gaussian distribution

$$f(r_i) = \frac{1}{\sqrt{2\pi\sigma^2}} \exp\left(-\frac{r_i^2}{2\sigma^2}\right) \tag{4}$$

with a mean of $\mu = 0$ and width of $\sigma = [2D(E)t]^{\frac{1}{2}}$.
The simulation uses the derived diffusion coefficients $D(E)$ by Ziegler (2014) for a purely turbulent magnetic field of 50 µG. Separated into two energy regimes the energy dependence of the diffusion coefficient follows a power law

$$D(E) = D_{10} \left(\frac{E}{10\,\mathrm{GeV}} \right)^{\delta} \tag{5}$$

where D_{10} represents the value of the diffusion coefficient $D(E)$ at 10 GeV (see Figure 2).

3.3 The proton distribution

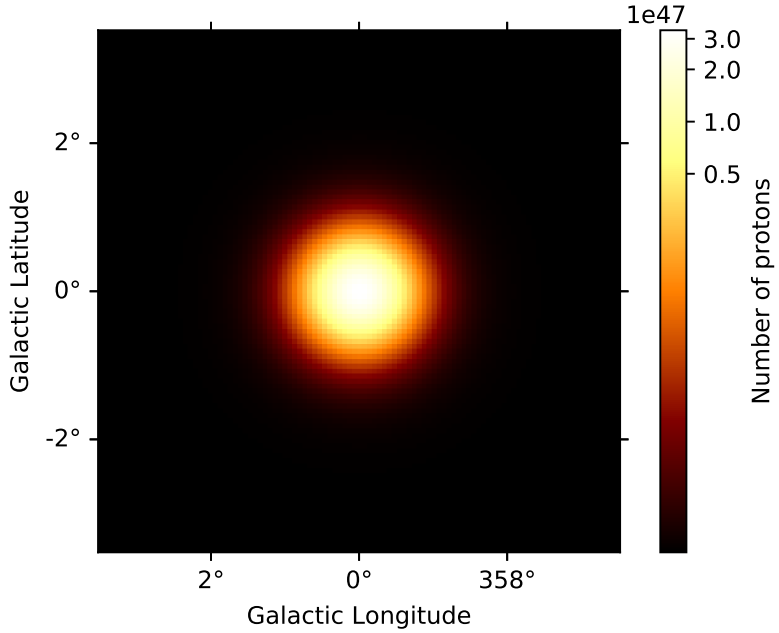

Figure 3: Simulated proton distribution projected to the Galactic plane. This was generated using a tracking time of 10^7 years. Particle loss due to interactions with the molecular clouds were not taken into account.

The input proton spectrum and the diffusion process in the simulation follow the work of Ziegler (2014). The calculation for the number of protons for an energy interval of 10^{-1} TeV to 10^5 TeV based on the estimate given by Aharonian et al. (2006) is adopted. Thus, 4.5×10^{49} protons are distributed according to the differential energy spectrum shown in Equation 1 over the energy range of

10^{-1} TeV to 10^{5} TeV partitioned into 300 bins equally spaced on a logarithmic scale. The spatial binning contains 105 bins in each direction to cover a range from -525 pc to 525 pc or $-3.5°$ to $3.5°$ respectively. The total tracking time was set to 10^{7} years while keeping discrete time steps of $\Delta t = 50$ yr.

For the diffusion process the derived diffusion coefficients D_{10} and indices δ from Ziegler (2014) for purely turbulent magnetic fields of 50 µG are adopted and the diffusion process is handled in the same way. However the code by Wong (2019) that is used in this thesis does not factor in particle losses due to the interaction with the molecular clouds as they are deemed insignificant. As was expected from Equation 4, this produces a Gaussian proton distribution shown in Figure 3.

3.4 Interaction process with the density map of molecular clouds

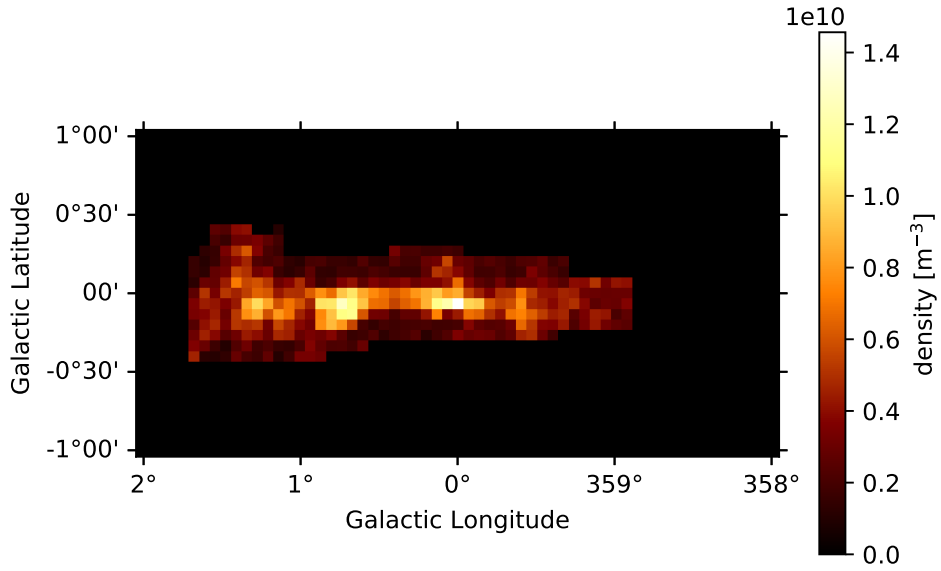

Figure 4: Density map of molecular clouds constructed by Ziegler (2014) based on the work of Nekrassov (2010) projected on the Galactic plane. The integrated density along the line-of-sight axis is represented by the color scale in units of m^{-3}. The non-projected map will later be used to calculate the γ-ray flux.

No changes were made to the density map of molecular clouds that was constructed by Ziegler (2014) based on the work of Nekrassov (2010). The map is shown in Figure 4 and Figure 5 with a projection to the line-of-sight axis and a projection perpendicular to the line-of-sight axis respectively. For the later analysis with `gammapy` a γ-ray flux cube is needed. In order to obtain the gamma-ray flux map with an energy axis produced by the interaction between proton-distribution and the density map of molecular clouds, the diffusion process is calculated for protons in the first energy bin. Afterwards the resulting proton distribution is multiplied by the density map elementwise and projected to the line-of-sight axis.

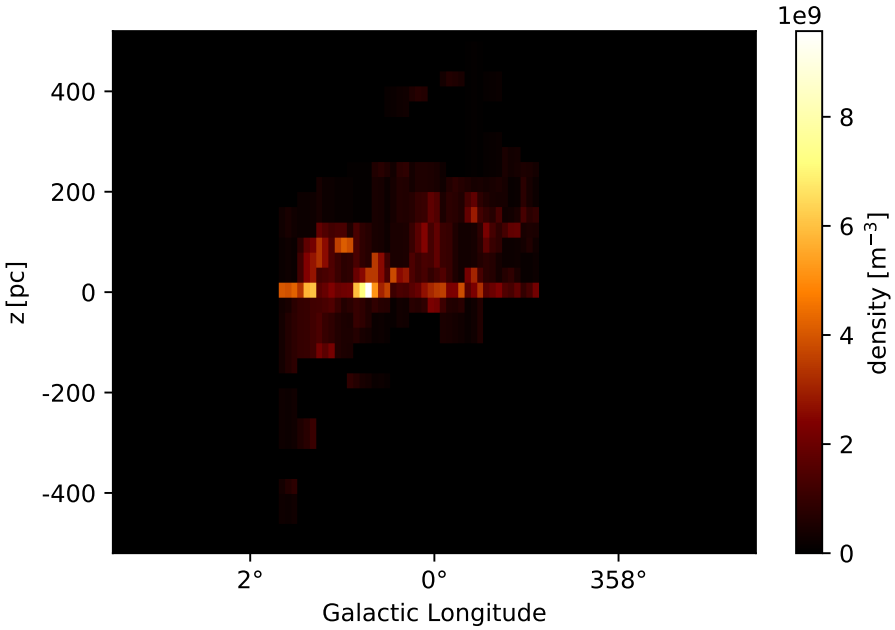

Figure 5: Density map of molecular clouds constructed by Ziegler (2014) integrated over Galactic Latitude using a face-on velocity distribution from Sawada et al. (2004). The color scale represents the density in units of m^{-3}. The non-projected map will later be used to calculate the γ-ray flux.

To get the γ-ray flux a two-dimensional look-up table developed by Ziegler (2014) based on the results given in Kelner et al. (2006) is used. This table contains the resulting flux $\mathrm{d}\Phi(E_\gamma, E_p)$ in discrete energy bins. A γ-ray flux cube along the line-of-sight can then be determined for the first proton energy bin. To get the complete γ-ray flux map this process is repeated for all 300 previously defined energy bins and the resulting maps are added up.

3.5 Simulation results

The γ-ray flux map produced by protons with an energy of 1 TeV can be seen in Figure 6. The produced γ-ray flux follows the distribution of the density map of molecular clouds, while the intensity decreases towards the outer regions.

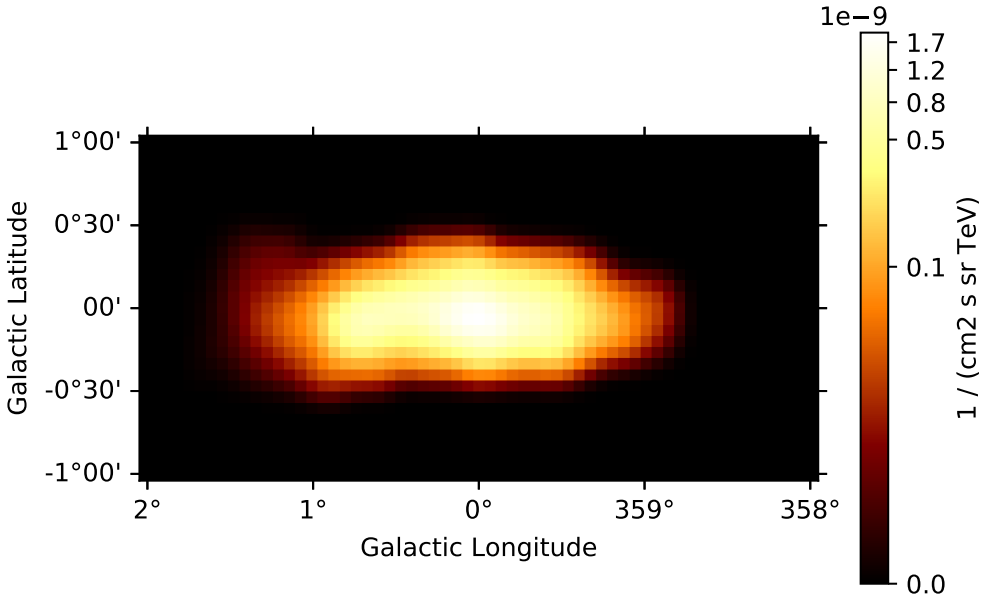

Figure 6: Simulated γ-ray flux map produced by protons with an energy of 1 TeV. The map was Gaussian smoothed with a radius of 0.08° to account for the H.E.S.S PSF and integrated over the line-of-sight axis. The distribution was generated from the code by Wong (2019) using a tracking time of 10^7 years with diffusion coefficients for 50 µG found by Ziegler (2014). Particle loss due to interactions with the molecular clouds were not taken into account.

The complete γ-ray flux map for all proton energies in the considered range from 10^{-1} TeV to 10^5 TeV is gained simply by adding up the produced flux maps for each of the 300 energy bins. The result is shown in Figure 7.

Unsurprisingly higher flux values are again observed towards the Center because the interaction of protons with the molecular cloud material is more likely due to their distribution. The spatial shape roughly matches the expectations from the density map of molecular clouds.

While the complete γ-ray flux map in Figure 7 still looks very similar to the flux map produced for only a single proton energy bin, the difference in flux can be seen when comparing the color bars. Another interesting property of the γ-ray flux map is its energy spectrum, which can be extracted by summation over the spatial dimensions. This is shown in Figure 8.

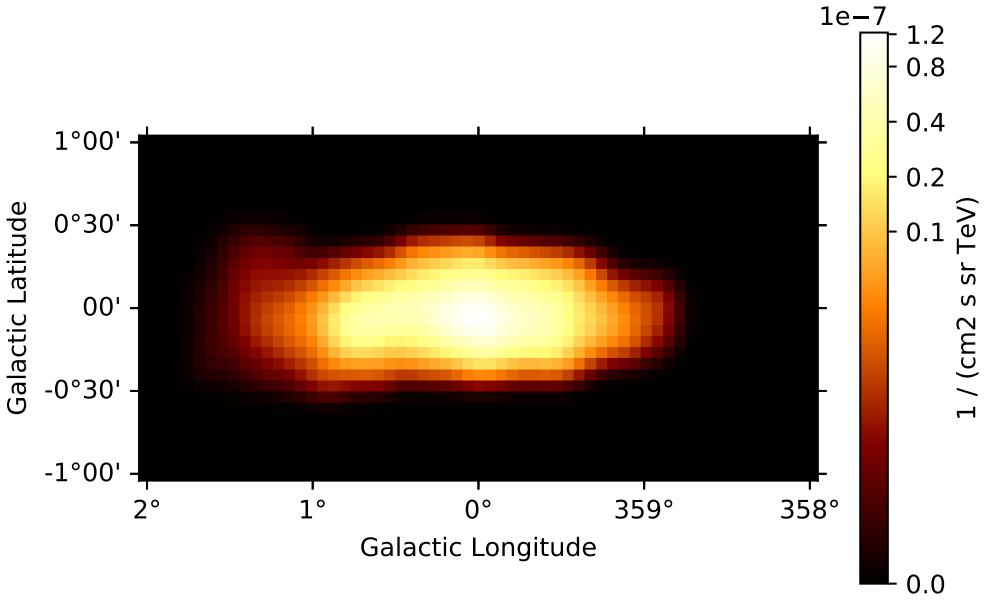

Figure 7: The full γ-ray flux map created by adding up the single proton energy flux maps. The map was Gaussian smoothed with a radius of 0.08° to account for the H.E.S.S PSF and integrated over the line-of-sight axis. Due to the used proton distribution the produced γ-ray flux is highest in the center.

For a later analysis with H.E.S.S data a power law is fit to the flux spectrum in an interval of 2×10^{-1} TeV to 8.4×10^{1} TeV. The result of a spectral index of ≈ 2.26 for the γ-ray spectrum suggests that the simulation produces a softer γ-ray spectrum compared to the input proton spectrum. The produced spectral index will be compared to the observed spectral index of the diffuse emission in the Galactic Center in subsection 4.4.

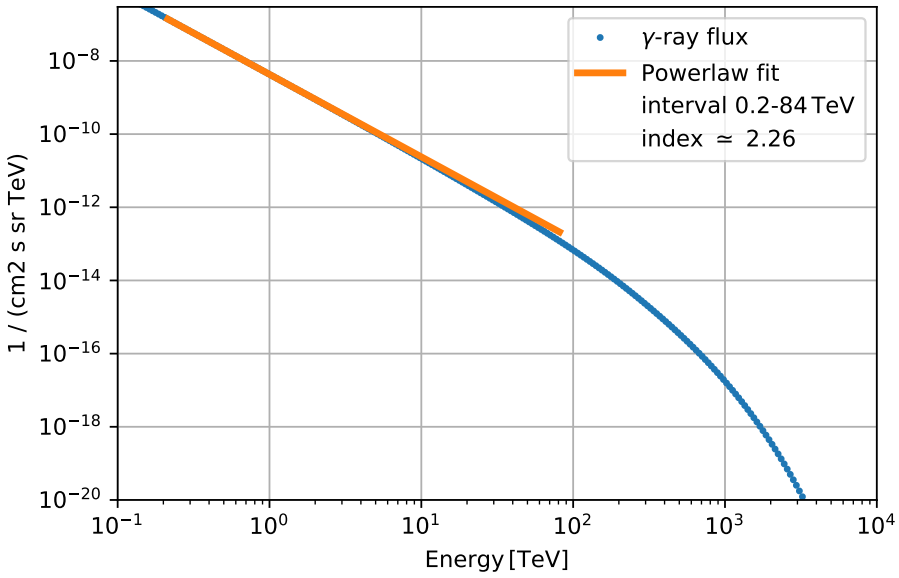

Figure 8: The γ-ray flux plotted as a function of energy created from the γ-ray flux map by summation over the spatial axes. The orange line represents a power law fit ($\Phi(E) = \Phi_0 \left(\frac{E}{\text{TeV}}\right)^{-\Gamma}$) in an interval of 2×10^{-1} TeV to 8.4×10^{1} TeV for a later analysis.

4 Using the model to analyse H.E.S.S data

The scenario that charged hadronic particles that were accelerated by a central source produce the diffuse γ-ray emission in the Galactic Center through interactions with the ambient matter is put to the test in this chapter. This is done by analysing 190 hours of H.E.S.S 1 data (gathered between 2004 and 2013) of the Galactic Center with the help of the `gammapy`-package for python. The idea is to model the background as well as known sources in the galactic center with the addition of the simulated γ-ray flux map as a model for the diffuse emission. The modeled sources include the super-massive black hole Sgr A*, the pulsar wind nebula G 0.9+0.1 and the gaussian source HESS J1745-303. The results are then compared to the data to check the validity of the model. Furthermore the obtained fit results for the point sources are compared to other publications.

4.1 Data configuration and background model preparation

For the analysis of the Galactic Center the same data set of 190 hours of dedicated observation of the Galactic Center region from the H.E.S.S 1 telescope are used

as in the work of Ruta (2019). In much the same way the thresholds for the used hadronic background model are calculated. This means that every observation has its own threshold as low as about 0.2 TeV applied, so that the analysable data is maximized. Because the sources and the diffuse model will be fit to the stacked counts map later, the background is fit separately from the other components at first to improve the stacked background model. Therefore the background is fit to each observation individually resulting in the right-hand plot in Figure 9. For a more accurate background estimation the central region with the three considered sources and the diffuse emission was excluded (see Figure 10). The pixel size of the observations is set to match the bin size of the diffuse model ($\approx 0.06°$) produced in section 3.

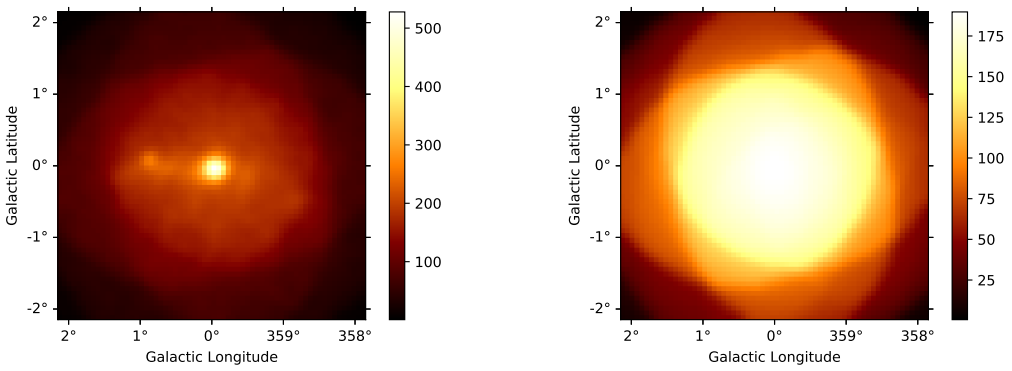

(a) (b)

Figure 9: **a,** γ-ray count map of the Galactic Center **b,** fitted background count map. Both plots are summed over the energy axis. The color scale of the count map is dimensionless and corresponds to 190 hours of H.E.S.S 1 data of the Galactic Center after applied background model thresholds covering an energy range from 2×10^{-1} TeV to 8.4×10^{1} TeV. Both plots are smoothed to account for the H.E.S.S PSF.

In Figure 10 the excess map is shown, which is computed by subtracting the two maps pictured in Figure 9 from each other. This time the right-hand plot shows excess map masked with the region that was used to fit the background. The masked map is reasonable flat, however there is still a visible hot spot area near the location of HESS J1745-303. Despite this unevenness there is no point in further increasing the volume of the excluded region because of the downside of having less data points for the background fit.

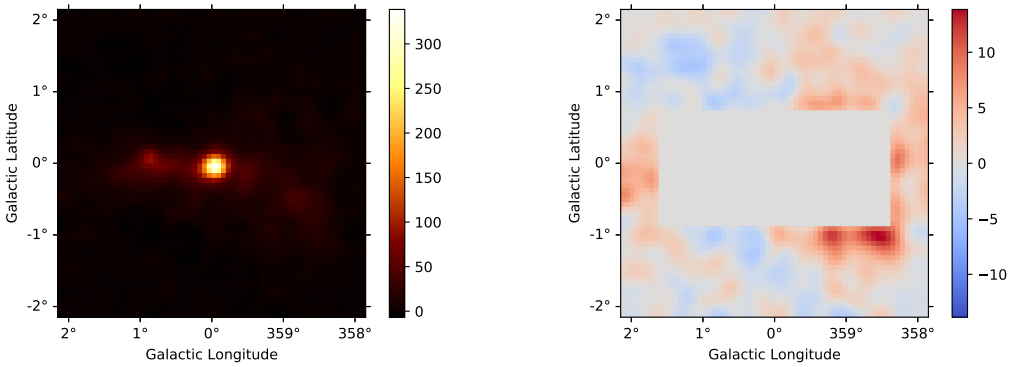

(a) (b)

Figure 10: **a,** excess map created from by subtracting the maps in Figure 9 from one another **b,** same excess map masked with the excluded region that was used to fit the background. The smoothing of the excess map was done after subtracting the unsmoothed counts and background map from each other. The masked excess map is reasonable flat supporting a proper background fit.

4.2 The source models

The considered sources for the fit are the super-massive black hole Sgr A*, the pulsar wind nebula G 0.9+0.1 and the Gaussian source HESS J1745-303. As the central source, Sgr A* seems to follow a power law with an exponential cutoff according to HESS Collaboration et al., 2016, pg. 13, whereas for G 0.9+0.1 no cutoff is needed [see Aharonian et al., 2005]. On that account the spectral models for these two sources are adopted. These two sources are fitted as point sources unlike HESS J1745-303 as this source is more spread out and therefore a Gaussian spatial model is preferred by the data. As with G 0.9+0.1 a power law is used as a spectral model for HESS J1745-303. The diffuse model that was described in section 3 is used as source model via the `gammapy`-package with only the normalization as a fit parameter.

4.3 The fit result

Using a mean energy dispersion and a mean point spread function with a maximum radius of 0.3° for all observations while refitting the stacked background model, the plots in Figure 11 are obtained. The corresponding parameters found to fit the data best are shown in Table 1 and Table 2.

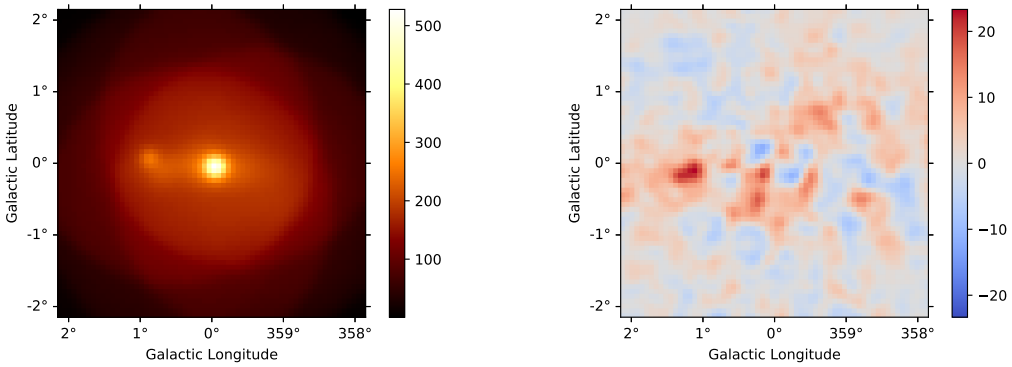

(a) (b)

Figure 11: **a,** Fit result using the source models for Sgr A*, G 0.9+0.1, HESS J1745-303 as well as the diffuse model that was presented in section 3 **b,** residual map obtained by subtracting the fit result from the original counts map seen on the left-hand plot in Figure 9. The smoothing of the residual map was done after subtracting the unsmoothed counts map and fit result from each other.

model	parameter	value	error	unit
Sgr A*	index	2.01e+00	2.01e-02	
	amplitude	2.80e-12	6.57e-14	$\mathrm{cm^{-2}\,s^{-1}\,TeV^{-1}}$
	lambda	1.18e-01	6.91e-03	$\mathrm{TeV^{-1}}$
G 0.9+0.1	index	2.49e+00	5.26e-02	
	amplitude	7.54e-13	3.78e-14	$\mathrm{cm^{-2}\,s^{-1}\,TeV^{-1}}$
HESS J1745-303	index	2.63e+00	4.45e-02	
	amplitude	8.63e-12	6.01e-13	$\mathrm{cm^{-2}\,s^{-1}\,TeV^{-1}}$
	sigma	4.76e-01	2.32e-02	degree
background model	norm	9.95e-01	1.39e-03	
	tilt	-2.88e-03	1.28e-03	
diffuse model	norm	9.56e+02	2.62e+01	

Table 1: Selected model parameters produced by fitting Sgr A*, G 0.9+0.1, HESS J1745-303, the diffuse model from section 3 and the stacked background in `gammapy` shown in Figure 11. The fit for the 3 source models and the background model is done with a reference of 1 TeV.

The energy spectra are fitted by a power law, $\Phi(E) = \Phi_0 \left(\frac{E}{\mathrm{TeV}}\right)^{-\Gamma}$, and a power law with an exponential cutoff, $\Phi(E) = \Phi_0 \left(\frac{E}{\mathrm{TeV}}\right)^{-\Gamma} \cdot \exp\left(-\lambda E\right)$. In both cases Φ_0 represents the amplitude and Γ the spectral index.

model	parameter	value	error	unit
Sgr A*	lon	-5.51e-02	1.18e-03	degree
	lat	-4.63e-02	1.21e-03	degree
G 0.9+0.1	lon	8.69e-01	1.96e-03	degree
	lat	7.62e-02	3.23e-03	degree
HESS J1745-303	lon	-1.32e+00	2.21e-02	degree
	lat	-5.61e-01	1.70e-02	degree

Table 2: Fitted coordinates for the sources Sgr A*, G 0.9+0.1, HESS J1745-303 given in the galactic coordinate frame, shown in Figure 11.

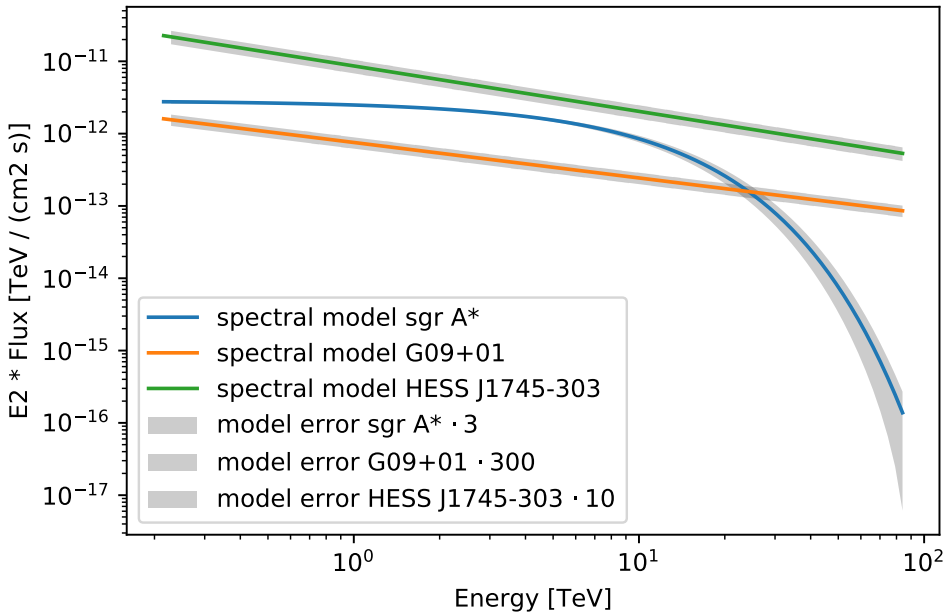

Figure 12: $E^2 \cdot \gamma$-ray flux plotted over energy for the best fit produced for Sgr A*, G 0.9+0.1 and HESS J1745-303. The energy range of 2×10^{-1} TeV to 8.4×10^{1} TeV is used to secure the validity of the background model. The model parameters used to produce this plot are found in the Table 1 and in the appendix (Table 4).

The cut-off energy is given by $\frac{1}{\lambda}$. For HESS J1745-303 the model parameter σ for the spatial model, $\Phi(\text{lon}, \text{lat}) = \frac{1}{2\pi\sigma^2} \exp\left(-\frac{1}{2}\frac{\theta^2}{\sigma^2}\right)$ where θ is the angular separation between the center of the Gaussian and the evaluation point, is shown, too.

For the central source Sgr A* a spectral index of ≈ 2.0 is found while the cut-off energy is about 8.5 TeV. For G 0.9+0.1 and HESS J1745-303 higher spectral indices of ≈ 2.5 and ≈ 2.6 respectively are found. For the Gaussian source HESS J1745-303 a sigma of $\approx 0.476°$ is reported, indicating a large spatial extent, however the uncertainty of the spatial position of this source is one order of magnitude higher compared to Sgr A* and G 0.9+0.1.

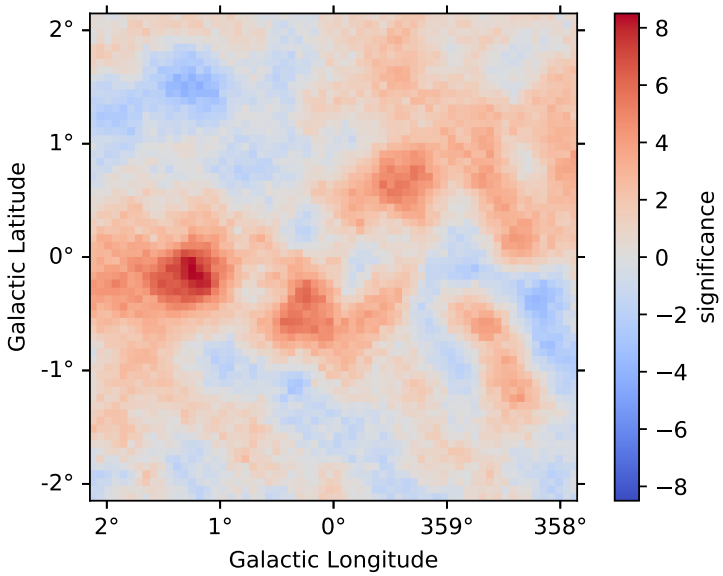

Figure 13: Li & Ma significance map obtained from the residual map shown in Figure 11 using a Top-hat filter with a radius of 0.24°. A high significance is found at a longitude of 1.25° and latitude of −0.15°.

Looking at the best best fit spectrum for the spectral model of the sources, see Figure 12, the model error for G 0.9+0.1 is surprisingly low. In comparison the model of Sgr A* has a higher uncertainty, especially for high energies. However as there are not as many data points for higher energies because of decreasing sensitivity of the H.E.S.S instrument in this energy range, this behaviour is expected. For energies less than 10 TeV the model uncertainty of Sgr A* is much lower, even undercutting the model uncertainty of HESS J1745-303. The energy range is chosen to cover an interval from 2×10^{-1} TeV to 8.4×10^{1} TeV as these are the needed boundaries for the background model to be valid.

The Li & Ma significance map of the fit (Figure 13) shows a very high significance at 1.25° longitude and −0.15° latitude. The pixel size of ≈ 0.06° results in a smoothed area of 0.24° which is significantly bigger than the HESS PSF, however even with a lower filter radius the detection of a possible source is clearly significant beyond statistical uncertainties. As the molecular cloud map for the diffuse model is clearly extending beyond a longitude of 1.25°, the high significance value could represent a possible source.

4.4 Comparison of the fit results

In order to get a first impression of the fit parameters the results will be compared to those found by other publications (see Table 3). For the super-massive black hole Sgr A* the results from HESS Collaboration et al. (2016) are used for comparison as a power law with an exponential cutoff was used for the spectral model, too. Furthermore the measured index of the diffuse emission can also be used for comparison. The spectral indices for G 0.9+0.1 and HESS J1745-303 are taken from Aharonian et al. (2005) and Aharonian et al. (2008).

source	spectral index	citation
Sgr A*	$2.14 \pm 0.02_{\text{stat}} \pm 0.02_{\text{syst}}$	HESS Collaboration et al., 2016, pg. 13
diffuse emission	$2.32 \pm 0.05_{\text{stat}} \pm 0.11_{\text{syst}}$	HESS Collaboration et al., 2016, pg. 13
G 0.9+0.1	$2.40 \pm 0.11_{\text{stat}} \pm 0.2_{\text{syst}}$	Aharonian et al., 2005, pg. 3
HESS J1745-303	$2.71 \pm 0.11_{\text{stat}} \pm 0.2_{\text{syst}}$	Aharonian et al., 2008, pg. 3

Table 3: Spectral indices for Sgr A*, G 0.9+0.1, HESS J1745-303 and the diffuse emission found by other publications. The spectral indices for the sources found in this thesis can be found in Table 1. There are only slight deviations for Sgr A* while G 0.9+0.1 and HESS J1745-303 are within the margin of error. The spectral index of the diffuse emission is also very close to the one obtained through the simulation (see Figure 8).

While the approach for analysing HESS J1745-303 in Aharonian et al. (2008) is much more refined, the approximation of the source by a Gaussian distribution does produce a similar spectral index and is sufficient for the purpose of testing the diffusion model. The measured spectral index of the diffuse emission in the work of HESS Collaboration et al. (2016) is also very similar to the one found for the γ-ray flux map produced by the simulation (see Figure 8). In this context the slightly different result for the spectral index of Sgr A* may be caused by the overlap with the diffusion model.

4.5 Analysing the diffusion model in different energy regimes

In this chapter the fit will be analysed in different energy regimes. As the model of the diffuse emission for the Galactic Center which was introduced in section 3 is particularly interesting, the focus is set on small cutouts of the Galactic Center.

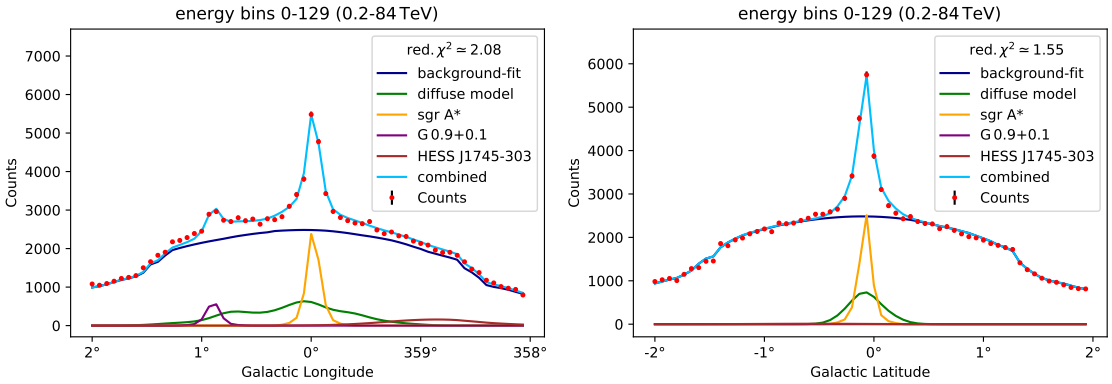

(a) (b)

Figure 14: **a,** Cutout of 4.0° longitude and 0.5° latitude of the counts and model map integrated over latitude **b,** Cutout of 0.5° longitude and 4.0° latitude of the counts and model map integrated over longitude. The separate model components and the combined model is shown. Both plots cover the full energy range of 2×10^{-1} TeV to 8.4×10^{1} TeV. For the errorbars the RMSE was used.

Two cutouts were made with the central coordinate being the location of Sgr A*. The first one covers a range of 4.0° longitude and 0.5° latitude, while the extent from the second one is 0.5° longitude and 4.0° latitude. The obtained maps are then integrated in latitude and longitude respectively and the different model components are plotted. This is shown Figure 14 for the whole energy range of 2×10^{-1} TeV to 8.4×10^{1} TeV.
The reduced χ^2 value is computed via the formula

$$\text{red. } \chi^2 = \frac{1}{\#\text{bins}} \sum_{\#\text{bins}} \frac{(\text{counts} - \text{combined})^2}{\text{counts}}$$

as the root-mean-square error (RMSE) was plotted as error bars. For the whole energy range this results in a red. χ^2 of 2.08 and 1.55 for the latitude and longitude integrated map respectively, see Figure 14. Looking at the contributing sources only Sgr A* can be seen in Figure 14**b** as G 0.9+0.1 and HESS J1745-303 are

located outside the central region from $-0.25°$ to $0.25°$ in longitude. Also worth noting is that the shape of the used diffuse model in this plot is similar to that of a slightly off-centered Gaussian distribution. In contrast Figure 14**a** shows a contribution by all model components, despite that the full extent of HESS J1745-303 is not covered by the cutout of $4.0°$ longitude and $0.5°$. Here, the shape of the diffusion model roughly follows the expectations from the used γ-ray flux map (Figure 7).

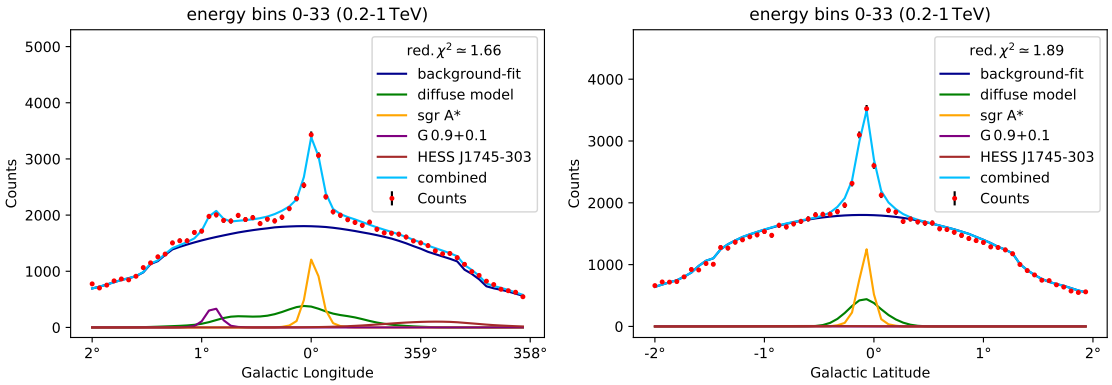

(a) (b)

Figure 15: **a,** Cutout of $4.0°$ longitude and $0.5°$ latitude of the counts and model map integrated over latitude **b,** Cutout of $0.5°$ longitude and $4.0°$ latitude of the counts and model map integrated over longitude. The separate model components and the combined model is shown. Both plots cover an energy range of 2×10^{-1} TeV to 1 TeV. For the error bars the RMSE was used.

There are improvements to the red. χ^2 when only the lower end of the energy range (2×10^{-1} TeV to 1 TeV) is taken into account (see Figure 15). While the regarded energy range is near the lower threshold of the background model, the contribution by its model component still fits the data quite well. In Figure 15**a** at around $0.4°$ longitude and $1.3°$ longitude there are slight deviations from the model, however these are not significant enough to leave much room for interpretation.
Looking at the energy range from 1 TeV to 3 TeV shown in Figure 16, the computed red. χ^2 values stay at the same level. While there is a decrease in counts, the source components start to have more impact compared to the background model when going to higher energies. Interestingly in Figure 16**a** the slight difference between the model and the observed counts at $1.3°$ longitude still persists while the deviation at $0.4°$ longitude does not. This hints at the high significance found in that region that are shown in Figure 13.

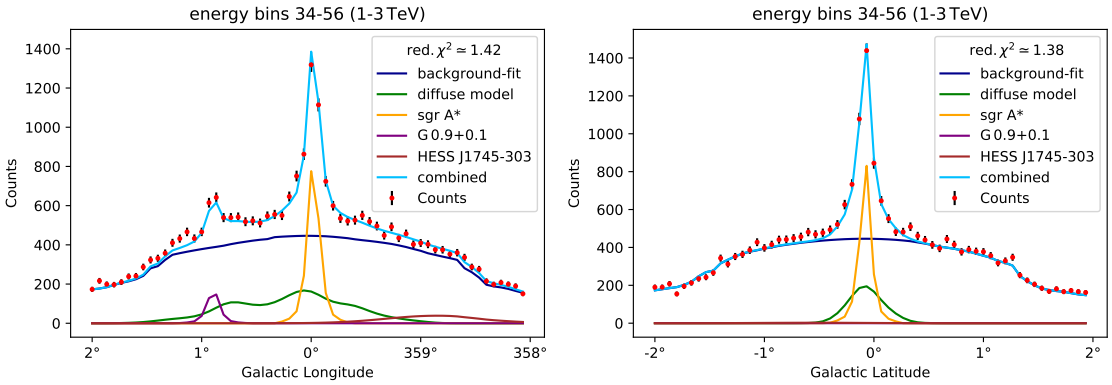

(a) (b)

Figure 16: **a,** Cutout of 4.0° longitude and 0.5° latitude of the counts and model map integrated over latitude **b,** Cutout of 0.5° longitude and 4.0° latitude of the counts and model map integrated over longitude. The separate model components and the combined model is shown. Both plots cover an energy range of 1 TeV to 3 TeV. For the error bars the RMSE was used.

As previously noted going from the energy range of 1 TeV to 3 TeV to a range of 3 TeV to 10 TeV comes with a significant decrease in counts (see Figure 17). As a result the error bars produced by applying a RMSE are now clearly visible. The resulting values for the red. χ^2 are very close to 1 for this energy range, suggesting that the extent of the match between the observations and estimates is in accord with the error variance at least in the considered region. In Figure 17**a** the contribution of the diffuse model is now visible beyond the location of G 0.9+0.1.

For very high γ-ray energies the sensitivity of the H.E.S.S instrument is declining and even less counts are registered from the observations. For this reason there is no point in looking at energies up to the threshold of the background model of 84 TeV. Therefore the highest energy range to be analysed is chosen to be 10 TeV to 30 TeV (see Figure 18). The plot features only data below 100 counts further increasing the relative size of the error bars. The resulting red. χ^2 values are increased, even reaching ≈ 2 for Figure 18**b**. It's worth noting that the diffusion model seems to be more spread out for higher energies compared to lower energies, which can be seen in Figure 18**a**. However since the counts also vary with energy this relation can not be proven right away.

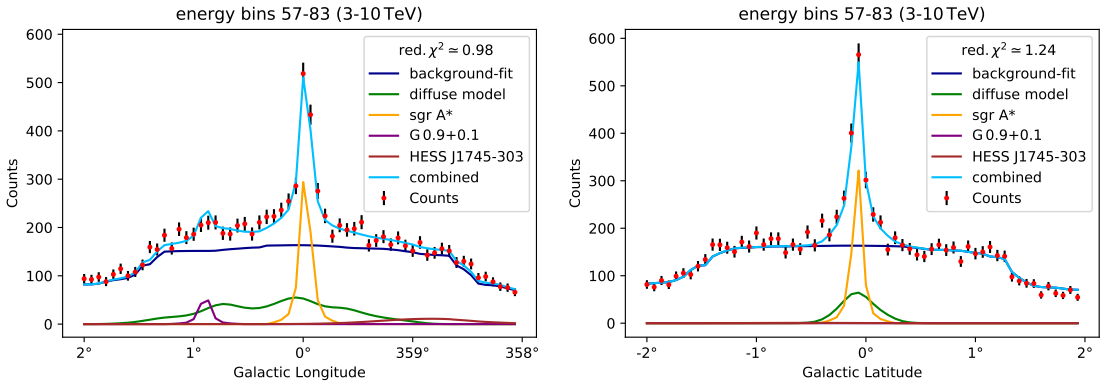

(a) (b)

Figure 17: **a,** Cutout of 4.0° longitude and 0.5° latitude of the counts and model map integrated over latitude **b,** Cutout of 0.5° longitude and 4.0° latitude of the counts and model map integrated over longitude. The separate model components and the combined model is shown. Both plots cover an energy range of 3 TeV to 10 TeV. For the error bars the RMSE was used.

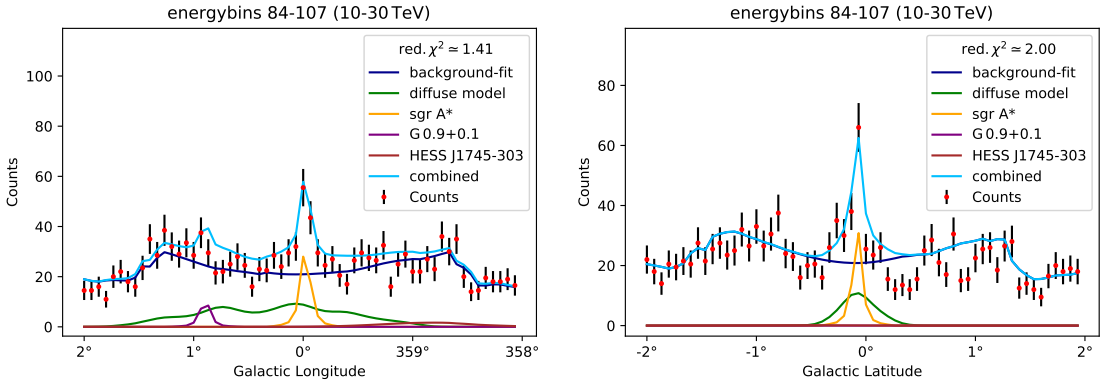

(a) (b)

Figure 18: **a,** Cutout of 4.0° longitude and 0.5° latitude of the counts and model map integrated over latitude **b,** Cutout of 0.5° longitude and 4.0° latitude of the counts and model map integrated over longitude. The separate model components and the combined model is shown. Both plots cover an energy range of 10 TeV to 30 TeV. For the error bars the RMSE was used.

In order to compare the diffusion model component for different energies, they need to be on the same scale. Therefore after extracting the model component a normalization is done. This is achieved by dividing the model by the integral over longitude or latitude, thus fixing the area under the curve to 1 for all energies. This leads to the plots shown in Figure 19 and Figure 20.

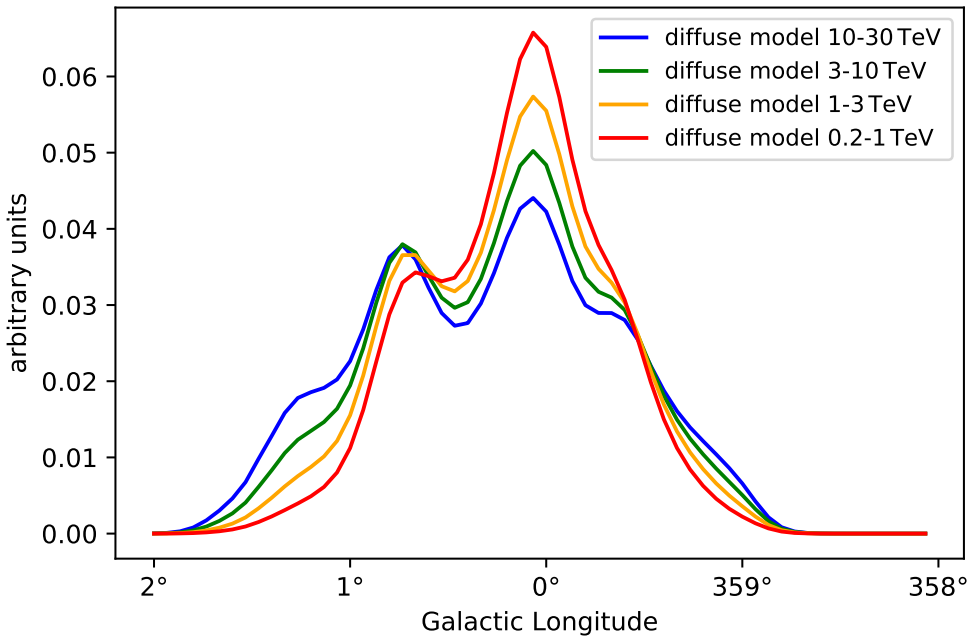

Figure 19: Comparison of the diffusion model components for different energy intervals in Galactic Longitude. The area under the curves was fixed to 1 for all energies. The diffuse model is more spread out for higher γ-ray energies as these tend to be produced by high energy protons which diffuse faster than low energy protons.

The difference between the diffusion model components from each energy interval in Galactic Longitude is clearly visible. Especially at a Galactic Longitude of 1.3° the difference is quite high due to the high density of molecular material in that area. In Galactic Latitude the diffusion model does not change significantly because of the cutout region of 0.5° longitude and 4.0° latitude. The molecular cloud density in this region is much more centered around 0° latitude and therefore almost all γ-rays are produced within a latitude of $\pm 0.5°$ latitude.

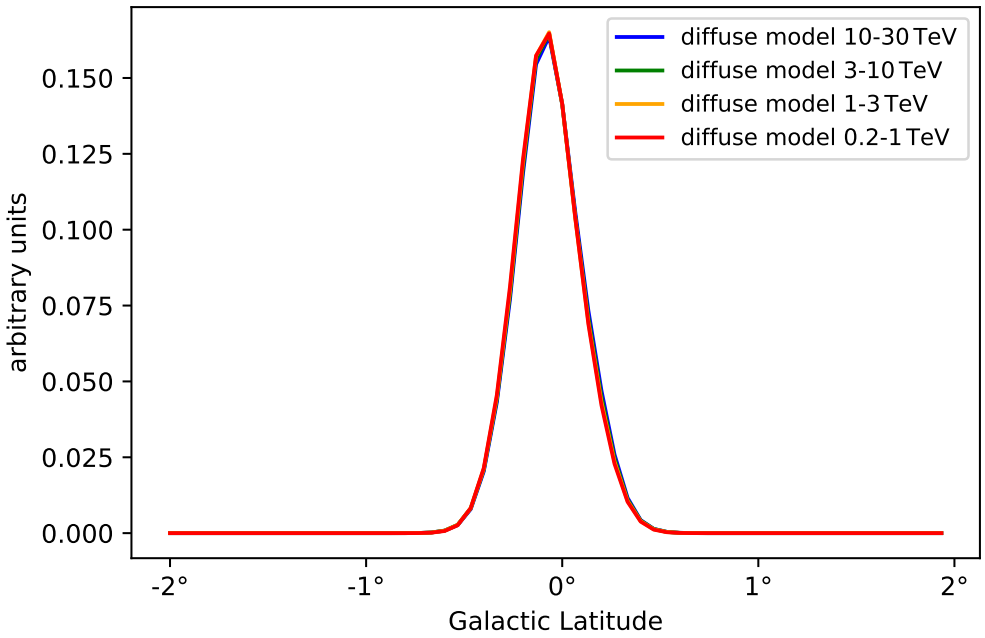

Figure 20: Comparison of the diffusion model components for different energy intervals in Galactic Latitude. The area under the curves was fixed to 1 for all energies. There is no significant change in the diffusion model for different energies as the molecular cloud does not reach out that far in latitude compared to longitude.

5 Conclusion and Outlook

In this thesis a simulation to model the observed diffuse γ-ray emission from the Galactic Center was developed together with Wong (2019) assuming the hadronic diffusion scenario as its origin. The simulation used the diffusion constant for 50 µG found by Ziegler (2014) with a tracking time of 10^7 years while particle losses due to the interaction with the molecular clouds were not accounted for. The differential energy spectrum of the protons was assumed to follow a power law with a spectral index of $\Gamma_p = 2$. The produced γ-ray flux map, which yields a spectral index of ≈ 2.26, was then used as a model for the diffuse γ-ray emission and fit to 190 hours of H.E.S.S 1 data together with source models for three dominant sources in the Galactic Center (Sgr A*, G 0.9+0.1 and HESS J1745-303). In the end the different model components were shown at different energy intervals with a focus on the developed diffuse emission model.

The results show that with the diffusion hypothesis of high-energy protons in the Galactic Center the observed diffuse emission can certainly be reproduced to some extent. The model used here does not claim to be a physically accurate representation of the processes in the Galactic Center but it does strongly favor that diffuse emission is produced by proton-proton interactions. Compared to the analysis of H. E. S. S. Collaboration et al. (2018) there is no need for a pronounced central component as this is now part of the diffuse emission model. Furthermore the results also support the possibility proposed by HESS Collaboration et al. (2016) that Sgr A* could have been more active over the last 10^{6-7} years, and therefore can be considered as an alternative to supernova remnants as a source of PeV Galactic cosmic rays. The spectral indices for the sources in this thesis are similar to the ones found by other publications, however the significance map (Figure 13) shows the possibility of another source located at about a longitude of 1.25° and latitude of -0.15° near the center of the massive molecular complex Sgr D. Another explanation for this excess could be that the density of the molecular clouds in that area has been underestimated.

A further improvement of the approach in this thesis is also possible, since the initial parameters for the simulations can be changed. This does apply for the diffusion coefficients as they could be changed e.g. to account for a stronger turbulent magnetic field in the Galactic Center as well as the index of the proton energy spectrum and the total tracking time. This is also a great opportunity to include data of the new H.E.S.S. II telescope.

Appendix

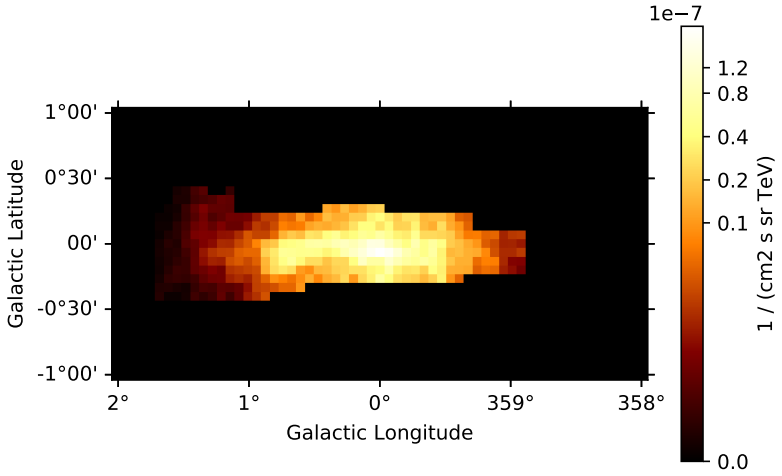

Figure 21: The full γ-ray flux map created by adding up the single proton energy flux maps. The map was integrated over the line-of-sight axis. Due to the used proton distribution the produced γ-ray flux is highest in the center.

source model	covariance	index	amplitude	lambda
Sgr A*	index	4.02e-04	1.61e-16	-4.05e-05
	amplitude	1.61e-16	4.32e-27	1.56e-16
	lambda	-4.05e-05	1.56e-16	4.77e-05
G 0.9+0.1	index	-2.95e-04	4.19e-16	
	amplitude	3.72e-17	5.58e-296	
HESS J1745-303	index	-4.99e-05	5.94e-17	
	amplitude	4.11e-15	-7.14e-27	

Table 4: Covariance for the spectral model parameters produced by the fit. These are used to produce the model error in Figure 12.

Bibliography

References

F. Aharonian, A. G. Akhperjanian, K. M. Aye, A. R. Bazer-Bachi, M. Beilicke, W. Benbow, D. Berge, P. Berghaus, K. Bernlöhr, C. Boisson, O. Bolz, and et al. Very high energy gamma rays from the composite SNR G 0.9+0.1. *Astronomy & Astrophysics*, 432(2):L25–L29, Mar 2005. doi: 10.1051/0004-6361:200500022.

F. Aharonian, A. G. Akhperjanian, A. R. Bazer-Bachi, M. Beilicke, W. Benbow, D. Berge, K. Bernlöhr, C. Boisson, O. Bolz, and et al. Discovery of very-high-energy γ-rays from the galactic centre ridge. *Nature*, 439(7077):695–698, 2006.

F. Aharonian, A. G. Akhperjanian, U. Barres de Almeida, A. R. Bazer-Bachi, B. Behera, M. Beilicke, W. Benbow, K. Bernlöhr, C. Boisson, O. Bolz, and et al. Exploring a SNR/molecular cloud association within HESS J1745-303. *Astronomy & Astrophysics*, 483(2):509–517, May 2008. doi: 10.1051/0004-6361:20079230.

Oleg G. Bakunin. *Turbulence and Diffusion*. Springer-Verlag Berlin Heidelberg, 1 edition, 2008. ISBN 978-3-540-68221-9.

gammapy. `https://gammapy.org`. (Version 0.12).

H. E. S. S. Collaboration, H. Abdalla, A. Abramowski, F. Aharonian, F. Ait Benkhali, A. G. Akhperjanian, T. Andersson, E. O. Angüner, M. Arakawa, M. Arrieta, and et al. Characterising the VHE diffuse emission in the central 200 parsecs of our Galaxy with H.E.S.S. *Astronomy & Astrophysics*, 612:A9, Apr 2018. doi: 10.1051/0004-6361/201730824.

HESS Collaboration, A. Abramowski, F. Aharonian, F. Ait Benkhali, A. G. Akhperjanian, E. O. Angüner, M. Backes, A. Balzer, Y. Becherini, J. Becker Tjus, and et al. Acceleration of petaelectronvolt protons in the Galactic Centre. *Nature*, 531(7595):476–479, Mar 2016. doi: 10.1038/nature17147.

S. R. Kelner, F. A. Aharonian, and V. V. Bugayov. Energy spectra of gamma rays, electrons, and neutrinos produced at proton-proton interactions in the very high energy regime. *Phys. Rev. D*, 74:034018, Aug 2006. doi: 10.1103/PhysRevD.74.034018. URL `https://link.aps.org/doi/10.1103/PhysRevD.74.034018`.

D. Nekrassov. *A detailed study of the H.E.S.S. data from the Galactic Center region*. Dissertation, Combined Faculties for the Natural Sciences and for Mathematics, Ruperto-Carola University, Heidelberg, Germany, 2010.

M. Ruta. H.E.S.S Data Analysis of the Galactic Center Region. Bachelor's thesis, 2019.

Tsuyoshi Sawada, Tetsuo Hasegawa, Toshihiro Handa, and R. J. Cohen. A molecular face-on view of the Galactic Centre region. *Monthly Notices of the Royal Astronomical Society*, 349(4):1167–1178, 04 2004. ISSN 0035-8711. doi: 10.1111/j.1365-2966.2004.07603.x. URL https://doi.org/10.1111/j.1365-2966.2004.07603.x.

Y. W. Wong. Personal communication, 2019.

A. Ziegler. Simulation of diffusive particle propagation and related γ-ray emission from proton-proton interactions at the galactic center. Master's thesis, Friedrich-Alexander-Universität Erlangen-Nürnberg, Erlangen Centre for Astroparticle Physics Physikalisches Institut 1 Lehrstuhl für Astroteilchenphysik, 2014.

Danksagung

An dieser Stelle möchte ich mich bei all denjenigen bedanken, die mich während der Anfertigung dieser Bachelorarbeit unterstützt und motiviert haben. Vielen Dank an

- Prof. Dr. Christopher van Eldik für die Vergabe dieses sehr interessanten Themas und die Betreuung dieser Bachelorarbeit. Besonders bei der Fehlersuche brachten die vielen Diskussionen mit Ihnen mich immer auf den richtigen Weg.
- Prof. Dr. Stefan Funk für die Übernahme des Zweitgutachtens.
- Yu Wun Wong für die Entwicklung des python-codes und die vielen hilfreichen Diskussionen über die Simulation sowie die Korrekturvorschläge für meine Arbeit.
- die gesamte Galactic Center Gruppe. Das Feedback in den wöchentlichen Treffen war immer sehr nützlich und motivierend. Lars und Dima gilt ein besonderer Dank für die Hilfe und das Beantworten vieler Fragen, vor allem in der Anfangsphase der Arbeit.
- meine Bürokollegen die immer für eine gute Stimmung sorgten. Ein besonderer Dank gilt Olaf für seine Unterstützung als LaTeX-Veteran sowie Matei und Freddy die mich auch außerhalb des Büros bei Laune hielten.
- Johannes Veh für die schnelle Hilfe bei technischen Schwierigkeiten.
- meine Familie für die Unterstützung beim Studium.
- meinen Bruder Oliver für das Korrekturlesen der Arbeit.

Erklärung

Hiermit bestätige ich, dass ich diese Arbeit selbstständig und nur unter Verwendung der angegebenen Hilfsmittel angefertigt habe.

Erlangen, den 30. Juli 2019

Martin Schneider